Comparison of an Fe Boltzmann temperature Lidar with a Na narrow-band lidar

George C. Papen and Daniel Treyer

The modeled performance of an Fe Boltzmann temperature lidar system is compared with existing Na narrow-band temperature techniques. The Fe Boltzmann technique employs mesospheric Fe as a fluorescence tracer and relies on the temperature dependence of the population difference of two closely spaced Fe transitions. The relative performance of the new technique is compared with an existing Na narrow-band temperature technique, and a link analysis is performed with measured data for both Na and Fe. It is shown that for currently available laser technology the two systems yield similar performance but the Fe system allows for the use of more broadband lasers. © 1998 Optical Society of America

OCIS codes: 280.0280, 280.3640, 010.3640.

1. Introduction

The study of global climate change requires knowledge about the lower atmosphere, as well as the middle and upper atmospheres. Because the middle atmosphere is inaccessible to aircraft, balloons, and most satellites, it is the most difficult region to study, and thus our current knowledge about this region's natural variability as a function of latitude, season, and solar cycle is poor. Currently, narrow-band temperature lidar techniques based on Na[1] and K[2,3] are some of the most accurate tools for probing the middle atmosphere. Unfortunately, the demanding operational requirements of these systems do not allow their use at remote sites or in aircraft. For global-scale observations of the temperature structure of the middle atmosphere, more robust lidars must be developed.

A recently proposed technique that might overcome this operational complexity and lead to more robust temperature systems employs mesospheric Fe as a fluorescence tracer.[4] It relies on the temperature dependence of the population difference of two closely spaced Fe transitions. The principal advantage of this technique is that the laser(s) can be broadband relative to narrow-band systems. This allows the use of more rugged and reliable lasers than with current systems. Lidars that employ this Fe broadband technique therefore can be operated under less demanding operational conditions.

In this paper we describe the design of an Fe Boltzmann temperature lidar currently under construction at the University of Illinois. The system consists of two independent and continuously operating lidar channels for probing two closely spaced Fe transitions. One channel operates at 372 nm, and one channel operates at 374 nm. Each channel consists of a 4-W injection-seeded, frequency-doubled alexandrite laser and a photon-counting receiver.[5] After an introduction to the two-frequency Na narrow-band temperature technique, an existing narrow-band temperature system is quantitatively compared with the broadband Fe system currently under development.

2. Na Narrow-Band Technique

Both the Fe technique and the Na technique rely on resonance fluorescence. The atmospheric response for such systems is described by the following lidar equation[6]:

$$N_t(z, t) = \frac{C}{z^2}\,\sigma_{\text{eff}}(f, T, v_R, g, I)\rho(z, t) + N_B, \qquad (1)$$

where

$$C = \eta\,\frac{T_a^{\,2} P_l \Delta z \Delta t}{(hc/\lambda)}\,\frac{A_R}{4\pi}. \qquad (2)$$

The authors are with the Department of Electrical and Computer Engineering, University of Illinois at Urbana-Champaign, 1406 West Green Street, Urbana, Illinois 61801. The email address for G. C. Papen is g-papen@uiuc.edu.

Received 3 April 1998; revised manuscript received 21 August 1998.

0003-6935/98/368477-05$15.00/0

© 1998 Optical Society of America

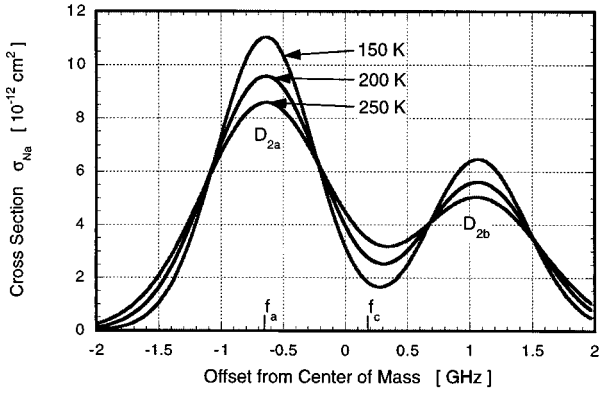

Fig. 1. Resonance fluorescence backscatter cross section of the Na D_2 transition as a function of frequency for several temperatures. A temperature increase causes the ratio $R_T = N_{f_c}/N_{f_a}$ to increase. The Na D_2 center wavelength is $\lambda_{Na} = 589.15826$ nm.

Equation (1) gives the total number of photons $N_t(z, t)$ detected by the lidar receiver from a column of thickness Δz at an altitude z over the time interval $(t, t + \Delta t)$. The variable $\rho(z, t)$ is the density of the tracer element. The variable C is a system constant that includes the one-way atmospheric transmittance T_a, laser power P_l, photon energy (hc/λ), and the solid angle of the scattering volume subtended by the receiver, $A_R/4\pi z^2$. The function $\sigma_{\text{eff}}(f, T, v_R, g, I)$ is the effective absorption cross section that depends on the laser frequency f, temperature T, radial wind velocity v_R, laser pulse line shape g, and intensity I. It is the integrated product of the laser line-shape function $g(f - f_l)$ and the thermally Doppler-broadened atomic line shape $\sigma(f, T, v_R, I)$. After subtraction of the background noise N_B from the total return counts, the signal $N = N_t - N_B$ is proportional to the effective-backscatter cross section.

Narrow-band resonance fluorescence temperature lidars exploit the temperature dependence of the absorption cross section of the tracer. The cross section of the Na D_2 line is depicted in Fig. 1 for several temperatures. As can be seen in Fig. 1, an increase in temperature results in a broadening of the line. We can measure the shape of the cross section by tuning a laser to selected frequencies within the absorption feature. For an accurate temperature measurement, the two laser frequencies are best chosen near the maximum (N_{f_a}) and near the minimum (N_{f_c}) of the absorption. This choice produces a large ratio that is highly sensitive to temperature changes but is insensitive to changes in wind velocity.[1] This choice also minimizes the sensitivity to frequency tuning errors, because the sensitivities to wind and frequency tuning errors are directly related.

For the two-frequency technique for temperature measurements, the ratio is

$$R_T(z, t) = \frac{N_{f_c}(z, t)}{N_{f_a}(z, t)} = \frac{\sigma_{\text{eff}}(f_c, T, v_R, g)\rho(z, t)}{\sigma_{\text{eff}}(f_a, T, v_R, g)\rho(z, t)}, \quad (3)$$

where f_a is a frequency near the peak of the Na D_{2a} resonance and f_c is near the local minimum. Differences in P_l, η, and A_R with the measurements of N_{f_a} and N_{f_c} can be calibrated by normalization of the return counts to the Rayleigh returns. In Eq. (3) it is assumed that N_{f_a} and N_{f_c} are measured simultaneously, and the response is linear with intensity.

To discuss system performance, one needs to relate the temperature accuracy ΔT to system parameters such as laser frequency, laser linewidth σ_l, or integration time Δt. To quantify this, we define the sensitivity as the normalized change in the ratio/degree of temperature change[6]:

$$S_T = \frac{(\partial R_T/\partial T)}{R_T}. \quad (4)$$

The sensitivity is a measure of the relative change of the ratio R_T with temperature, and for accurate temperature measurements, high sensitivity is required.

From the differential $\Delta T = \Delta R(\partial T/\partial R) = (\Delta R/R)/S_T$, the mean-square temperature error from uncertainty in the ratio is given by

$$\langle(\Delta T)^2\rangle = \frac{1}{(S_T)^2}\left\langle\left(\frac{\Delta R_T}{R_T}\right)^2\right\rangle. \quad (5)$$

The relative error in the ratio that is due to photon noise is calculated with the differential

$$\Delta R_T = \Delta N_{f_c}\frac{\partial R_T}{\partial N_{f_c}} + \Delta N_{f_a}\frac{\partial R_T}{\partial N_{f_a}} = R_T\left(\frac{\Delta N_{f_c}}{N_{f_c}} - \frac{\Delta N_{f_a}}{N_{f_a}}\right). \quad (6)$$

When we apply Poisson statistics [variance $(\Delta N_{f_i})^2 = N_{f_i}$] and note that the noise in N_{f_a} and N_{f_c} is uncorrelated $(\langle\Delta N_{f_a}\Delta N_{f_c}\rangle = 0)$, the mean-square relative error in the ratio that is due to photon noise becomes

$$\left\langle\left(\frac{\Delta R_T}{R_T}\right)^2\right\rangle = \frac{1}{N_{f_a}}\left(1 + \frac{1}{R_T}\right), \quad (7)$$

where $\langle\ \rangle$ denotes statistical average and background noise N_B is neglected. By substitution of Eq. (7) into Eq. (5), the rms temperature error that is due to photon noise becomes

$$\Delta T = \frac{1}{S_T}\left(\frac{1 + 1/R_T}{N_{f_a}}\right)^{1/2} = \frac{Q_T}{(N_{f_a})^{1/2}}. \quad (8)$$

The parameter $Q_T{}^2$ is the number of photon counts required at f_a for 1 K of temperature accuracy.

3. Fe Boltzmann Temperature Lidar Technique

The Fe Boltzmann technique relies on the temperature dependence of the ratio of the ground-state populations of two closely spaced Fe lines. At thermal equilibrium this ratio is the Boltzmann factor $\exp(\Delta E/kT)$.[4] The Fe system utilizes the 372- and the 374-nm transitions. The spectroscopic parameters are shown in Table 1. The cross sections of these two transitions are shown in Fig. 2. After sub-

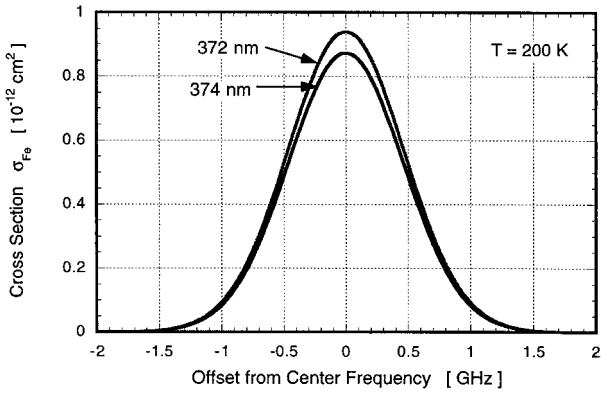

Fig. 2. Resonance fluorescence backscatter cross sections of the Fe 372- and Fe 374-nm transitions as a function of frequency. The center wavelengths are $\lambda_1 = 371.993$ nm and $\lambda_2 = 373.713$ nm.

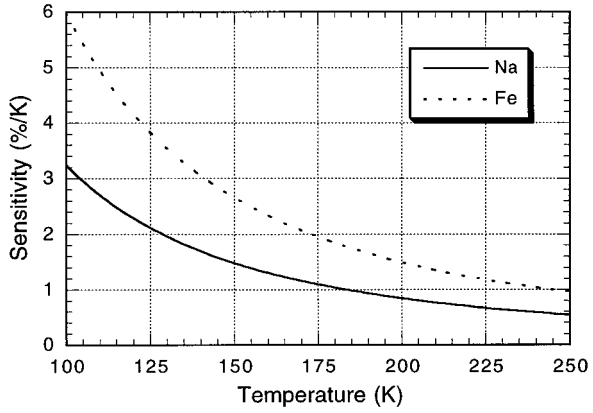

Fig. 3. Sensitivity of the ratio R_T for the Na narrow-band technique and the Fe Boltzmann technique. System parameters are listed in Table 2.

traction of the background noise, the ratio of the photon counts at the two wavelengths is

$$R_T = \frac{N_{374}}{N_{372}} = \frac{\sigma_2 \lambda_2 g_2}{\sigma_1 \lambda_1 g_1} \exp\left(-\frac{\Delta E}{kT}\right) = C_1 \exp\left(-\frac{C_2}{T}\right). \quad (9)$$

Here σ_i are the peak values of the effective Fe cross sections, λ_i are the center wavelengths of the Fe transitions, and g_i are degeneracies. The cross sections of the two transitions are Gaussian. Assuming that the laser line shape is also Gaussian, the effective-backscatter cross section becomes

$$\sigma_{\text{eff}}(f, T, \sigma_l) = \frac{1}{(2\pi\sigma_e^{\,2})^{1/2}} \exp\left[-\frac{(f - f_i)^2}{2\sigma_e^{\,2}}\right], \quad (10)$$

where f_i denotes the center frequency of a transition and the effective linewidth $\sigma_e^{\,2} = \sigma_l^{\,2} + \sigma_D^{\,2}$ is the geometric sum of the laser linewidth and the Doppler-broadened atomic linewidth.

At $T = 200$ K and $\sigma_l = 800$ MHz FWHM and with the values of the oscillator strength from Table 1, the peak values of the effective cross section are $\sigma_1 = 0.759 \times 10^{-16}$ m^2 and $\sigma_2 = 0.704 \times 10^{-16}$ m^2. Evaluating Eq. (9) with the values from Table 1, the constants are $C_1 = 0.725$ and $C_2 = 598.446$ K^{-1} and the ratio $R_T = 0.0364$. The sensitivity, as defined by Eq. (4), becomes

$$S_T = \frac{C_2}{T^2} \approx \frac{600}{T^2} \quad (11)$$

(at 200 K). The mean-square temperature error from uncertainty in the ratio $\langle(\Delta T)^2\rangle$, the mean-square error in the ratio that is due to photon noise $\langle(\Delta R_T/R_T)^2\rangle$, and the resulting rms temperature error that is due to photon noise ΔT are the same as given by Eqs. (5), (7), and (8), respectively, but with N_{f_a} replaced with N_{372} and N_{f_c} replaced with N_{374}.

Substituting Eq. (9) into Eq. (8) yields

$$Q_T = \frac{T^2}{C_2}\left[1 + \frac{1}{C_1}\exp\left(\frac{C_2}{T}\right)\right]^{1/2}. \quad (12)$$

At low temperatures the ratio R_T is high because the ground-state population of the 374-nm transition is small compared with the 372 line. The sensitivity, in contrast, is high at low temperatures, because a small temperature change yields a relatively large change in the ground-state population of the 374 transition, whereas the ground-state population of the 372 line remains relatively constant. However, there are few return counts N_{374} at low temperatures, and thus the photon noise of N_{374} is high. Owing to these two effects, temperature accuracy suffers at low and high temperatures, with an optimum at some intermediate temperature. This behavior is also reflected in the expression for Q_T, which is a measure for the number of required photons for a given temperature accuracy. The first effect described above is represented in Eq. (12) by the factor T^2 and the photon noise effect by the square root.

Table 1. Spectroscopic Parameters of the 372- and 374-nm Transitions[a]

λ (nm)	E_i (cm^{-1})	E_k (cm^{-1})	g_i	g_k	A_{ki} (10^8 s^{-1})	f_{ki}
371.993	0.0	26875	9	11	0.162	0.0412
373.713	415	27167	7	9	0.142	0.0381

[a] λ is the wavelength in nanometers, E_i is the initial energy level in centimeters to the power of −1, E_k is the final energy level in centimeters to the power of −1, g_i and g_k are the degeneracies of the two states, A_{ki} is the transition probability (10^8 s^{-1}), and f_{ki} is the oscillator strength (from Ref. 7).

4. Comparison

We now compare the performance of mesospheric temperature lidar systems, employing the two-frequency Na narrow-band technique and the Fe Boltzmann technique. The sensitivity (percentage change of the ratio R_T/unit temperature change) is

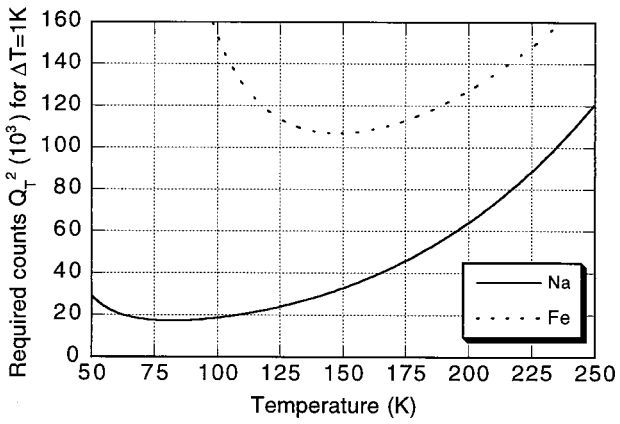

Fig. 4. Required number of return counts for 1 K temperature accuracy for the Na system and the Fe system.

shown in Fig. 3 as a function of temperature for both techniques. Over typical mesospheric temperatures (100–250 K) the sensitivity of the Na technique is approximately half of that of the Fe technique. For both techniques, as the temperature increases, S_T decreases. This occurs in the Na narrow-band technique because the cross section σ_{Na} becomes smoother, owing to Doppler broadening of the individual transitions Na D_{2a} and Na D_{2b} (see Fig. 1). For the Fe Boltzmann technique, S_T decreases with temperature, owing to an increase in the ground-state population of the 374-nm transition with respect to the 372-nm transition. In both cases the ratio approaches unity as the temperature increases, which decreases the sensitivity. To achieve 1 K accurate temperatures at $T = 200$ K, the ratio R_T must be known to a rms accuracy of 0.83% with the Na technique and to 1.5% with the Fe technique.

Figure 4 shows $Q_T{}^2$, the required number of return counts for a 1-K temperature accuracy for both the Na and the Fe systems. At low temperatures, Q increases because the photon error is dominated by the frequency that has the lowest signal and both N_{f_a} and N_{374} decrease. At high temperatures, Q increases because the sensitivity decreases. The quantity $Q_T{}^2$ is generally lower for the Na system than it is for the Fe system. At $T = 200$ K, $Q_T{}^2 = 64 \times 10^3$ for the Na system, whereas $Q_T{}^2 = 127 \times 10^3$ for the Fe system.

A significant difference between the two systems is their sensitivity to radial winds and to frequency tuning errors. As discussed below for the Na narrow-band temperature technique, the optimal frequencies for a temperature-only measurement are at the maximum and minimum of the absorption cross section. In practice the actual frequencies used deviate slightly from the ideal case, and this results in a residual sensitivity of 0.174 K ms^{-1} at a nominal radial wind velocity of 0 m s^{-1} for the system parameters listed in Table 2.[6] The sensitivity of the narrow-band technique to winds is used to make wind measurements with a different set of two frequencies on the wings of the D_{2a} line,[1] or both temperature and wind measurements can be made simultaneously with a three-frequency technique.[2]

In contrast to operational narrow-band Na systems, the nominal operating points for the broadband Fe system are at the optimal frequencies for insensitivity to winds and tuning errors. Furthermore, the use of a large laser linewidth implies that the effective cross section is significantly broader than the narrow-band system. The combination of these two effects results in a sensitivity of the temperature with respect to either the radial winds or tuning error that is extremely small (0.011 K ms^{-1} for a 50-MHz tuning error). This robust insensitivity to radial winds

Table 2. System Parameters Used in the Simulation of the Current Two-Frequency Na Narrow-Band System and the New Fe Boltzmann System

	Na Narrow-Band System	Fe Boltzmann System
Layer parameters[a]		
Transition wavelengths (air)	$\lambda_{NaD_2} = 589.15826$ nm	$\lambda_1 = 371.993$ nm $\lambda_2 = 373.713$ nm
Total abundance C_ρ	5.35×10^9 cm^{-2}	10.6×10^9 cm^{-2}
rms width σ_ρ	4.42 km	3.41 km
Peak density ρ_{pk}	4.83×10^9 m^{-3}	12.4×10^9 m^{-3}
Altitude z_{pk}	92.1 km	88.1 km
Atmospheric transmittance (one way) T_a	0.7	0.5
Laser parameters		
Effective backscatter cross section ($T = 200$ K)	$\sigma_{eff,f_a} = 9.49 \times 10^{-12}$ cm^2 $\sigma_{eff,f_c} = 2.80 \times 10^{-12}$ cm^2	$\sigma_{eff,1} = 0.759 \times 10^{-12}$ cm^2 $\sigma_{eff,2} = 0.704 \times 10^{-12}$ cm^2
Line width σ_l	60 MHz rms	800 MHz FWHM
Total power P_l	1 W	8 W (both lines)
Receiver parameters		
Receiver aperture A_R	0.130 m^2,[b] (%)	0.130 m^2 (%)
Receiver optics transmittance η_R	19	19
Detector quantum efficiency η_{QE}	11	28

[a]Annual mean at 40° N, Urbana, Illinois (from Ref. 8).
[b]0.099 m^2 actual.

also implies that the broadband Fe system cannot be used for wind measurements.

5. Link Analysis

To compare quantitatively the performance of the Fe Boltzmann system versus that of a Na narrow-band system, the respective integration times are ratioed:

$$r = \frac{\Delta t_{\mathrm{Fe}}(T, \Delta T, z)}{\Delta t_{\mathrm{Na}}(T, \Delta T, z)}. \tag{13}$$

The performance ratio r depends on the temperature accuracy, the temperature itself, and the position within the tracer layer. From Eqs. (1) and (2) the integration time is given by

$$\Delta t = 2\,\frac{N(T, \Delta T) z^2}{\sigma_{\mathrm{eff}}(T)\rho(z)}\,\frac{1}{\eta}\,\frac{(hc/\lambda)}{T_a^{\,2} P_l \Delta z}\,\frac{4\pi}{A_R}. \tag{14}$$

Here $N(T, \Delta T)$ is the required number of counts for a specified temperature accuracy ΔT at temperature T, obtained from Eqs. (8) and (12). If there is only one laser in a system, only half of the time can be spent at each frequency, which doubles the integration time. For a 1 K temperature accurate measurement at the altitude where the tracer layers have their peak density, the performance of the Fe system relative to the Na system is

$$r_{\mathrm{pk}} = \frac{Q_{\mathrm{Na}}^{\,2}(T)}{Q_{\mathrm{Fe}}^{\,2}(T)}\,\frac{z_{\mathrm{pk,Na}}^{\,2}}{z_{\mathrm{pk,Fe}}^{\,2}}\,\frac{\sigma_{\mathrm{eff,Fe}}(T)}{\sigma_{\mathrm{eff,Na}}(T)}\,\frac{\rho_{\mathrm{pk,Fe}}}{\rho_{\mathrm{pk,Na}}}\,\frac{\eta_{\mathrm{Fe}}}{\eta_{\mathrm{Na}}}\,\frac{\lambda_{\mathrm{Fe}}}{\lambda_{\mathrm{Na}}} \times \frac{T_{a,\mathrm{Fe}}^{\,2}}{T_{a,\mathrm{Na}}^{\,2}}\,\frac{P_{l,\mathrm{Fe}}}{P_{l,\mathrm{Na}}}\,\frac{A_{R,\mathrm{Fe}}}{A_{R,\mathrm{Na}}}. \tag{15}$$

For a practical system the total receiver efficiency η consists of the transmittance η_R of the receiver optics (including filters) and the quantum efficiency η_{QE} of the detector: $\eta = \eta_R \eta_{\mathrm{QE}}$. Table 2 lists the system parameters. The tracer density as a function of height is assumed to be Gaussian with the rms width σ_ρ and the peak density located at z_{pk}:

$$\rho(z) = \frac{C_\rho}{\sqrt{2\pi}\,\sigma_\rho}\exp\left[-\frac{(z - z_{\mathrm{pk}})^2}{2\sigma_\rho^{\,2}}\right]. \tag{16}$$

Here the factor leading the exponential is the peak density ρ_{pk}. Measured values for C_ρ, σ_ρ, and z_{pk} were taken from Ref. 8. The atmospheric transmittance is less for the Fe system, because of the absorption of ultraviolet light by ozone. Values for T_a were taken from Ref. 9. The photomultiplier tubes are assumed to be used as detectors. The detector quantum efficiency η_{QE} is larger for the Fe system, because of higher photon energy.

The main difference between the system parameters listed in Table 2 is that the Fe system power is assumed to be eight times that of the Na system power, because of the increase in linewidth tolerance for the Fe system and the availability of solid-state laser technology to produce the two Fe wavelengths. With the values from Table 2, for a 1 K accurate temperature measurement and column height $\Delta z = 3$ km, the integration times for the two systems become $\Delta t_{\mathrm{pk,Na}} = 389$ s and $\Delta t_{\mathrm{pk,Fe}} = 352$ s at $T = 200$ K. This results in a relative performance of the Fe versus the Na system of $r_{\mathrm{pk}} = 110\%$, thus indicating comparable system performance with current laser technology.

6. Conclusions

The broadband Fe Boltzmann system and the narrow-band Na system yield similar performance if the total power of the Fe system is approximately eight times that of the Na system. However, the Fe system has a significant practical advantage in that the laser linewidth tolerance for comparable performance can be an order of magnitude less than that for the Na system. It is also much less sensitive to wind or frequency tuning errors. However, this robust insensitivity also implies that the broadband Fe system cannot be used for wind measurements.

This study was supported by the National Science Foundation under grant NSF ATM96-12251.

References

1. R. E. Bills, C. S. Gardner, and C.-Y. She, "Narrowband lidar technique for sodium temperature and Doppler wind observations of the upper atmosphere," Opt. Eng. **30,** 13–21 (1991).
2. G. C. Papen, C. S. Gardner, and W. M. Pfenninger, "Analysis of a potassium lidar system for upper-atmospheric wind-temperature measurements," Appl. Opt. **34,** 6950–6958 (1995).
3. U. von Zahn and J. Hoffner, "Mesopause temperature profiling by potassium lidar," Geophys. Res. Lett. **23,** 141–144 (1996).
4. J. A. Gelbwachs, "Iron Boltzmann factor lidar: proposed new remote-sensing technique for mesospheric temperature," Appl. Opt. **33,** 7151–7156 (1994).
5. G. C. Papen and D. Treyer, "Comparison of an Fe Boltzmann lidar with a Na narrowband lidar," in *Proceedings of the 19th International Laser Radar Conference*, NASA Spec. Publ. SP-1998-207671/PT1 (NASA, Washington, D.C., 1998), pp. 355–358.
6. G. C. Papen, W. M. Pfenninger, and D. M. Simonich, "Sensitivity analysis of Na narrowband wind–temperature lidar systems," Appl. Opt. **34,** 480–498 (1995).
7. J. R. Fuhr, G. A. Martin, and W. L. Wiese, "Atomic transition probabilities: iron through nickel," J. Phys. Chem. Ref. Data **17,** 25 (1988).
8. T. J. Kane and C. S. Gardner, "Structure and seasonal variability of the nighttime mesospheric Fe layer at midlatitides," J. Geophys. Res. **98,** 16,875–16,886 (1993).
9. M. Bass, ed., *Handbook of Optics: Fundamentals, Techniques, and Design* (McGraw-Hill, New York, 1995), Chap. 44, p. 44-2.